Defence Science Journal, Vol. 70, No. 3, May 2020, pp. 249-259, DOI : 10.14429/dsj.70.14345

Study on Crush Tube's Geometric Cross-sections and Topology for Axial Crashworthiness

T.J. Reddy[#,*], V. Narayanamurthy[@], and Y.V.D. Rao[#]

[#]*Department of Mechanical Engineering, BITS-Pilani, Hyderabad - 500 079, India*
[@]*DRDO-Research Centre Imarat, Hyderabad - 500 069, India*
[*]*E-mail: janardhan.tjr@gmail.com*

ABSTRACT

Crush tubes are used as crash impact energy absorbing structure (EAS) and are located in the frontal compartment of road vehicles. Ideal crashworthiness of an EAS mandates that the equivalent decelerations due to impact forces should to be ≤ 20g; and crush force and stroke efficiencies should tend to unity. It is understood from the literature that no single geometric cross-section shape exhibits a near-ideal crashworthiness; and most EAS members exhibit a high initial peak crush force which is detrimental to the occupant safety, and moderate stroke and crush force efficiencies leading to a compromise in the total energy absorbed. In this paper, finite element analysis (FEA) methodology is formulated and experimentally validated for axial crush of a crush tube of SS304 material with circular cross section. Subsequently, plastic deformation phenomenon and folding patterns in relation to crush force behaviour of crush tubes with various basic cross-sections of polygonal geometric shapes from triangle to octagon and circle are extensively studied through FEA. Further, two new geometric cross-section profiles with combination of basic shapes are proposed to combine the merits of different basic shapes. The crashworthiness of all basic cross-sections including the two proposed cross-section profiles is assessed based on standard parameters. The proposed new geometries may form a basis for the development of new EAS configurations for enhanced crashworthiness.

Keywords: Crush tubes; Energy absorption; Crashworthiness; Crush force efficiency; Stroke efficiency; FEA

1. INTRODUCTION

Introduction of Highway Safety Act in the second half of the 20th century by USA has triggered the formulation of guidelines for vehicle manufacturers in several aspects of passenger safety. These safety regulations later came into existence as Federal Motor Vehicle Safety Standards (FMVSS) in USA and soon the other countries started enforcing similar standards and guidelines, as appropriate to their regions[1]. Crashworthiness and occupant safety have been given a top priority in vehicle engineering since then. Vehicle safety systems are designed to protect occupants during various collision scenarios (frontal, side, roll-over crashes or others). These collisions exhibit uniqueness in terms of the damage pattern to the vehicle and injuries to its occupants[1,2]. Crashworthiness with reference to frontal impact may be understood as the measure of vehicle's frontal energy absorbing structure's (EAS) capability to absorb the impact energy through controlled plastic deformation while avoiding intrusion of engine block into the passenger cell and keep the impact-induced decelerations within the human tolerance limits (crush forces within the allowable limits)[2,3].

Received : 26 March 2019, Revised : 04 April 2020
Accepted : 16 April 2020, Online published : 27 April 2020

The major sources of occupant's injury during an accident are[4]:

(i) High decelerations
(ii) Crushing of the occupant compartment and intrusion of heavy masses
(iii) Primary and secondary impacts with the vehicle interiors and
(iv) Ejection from the vehicle if the occupant is not belted.

The frontal collision is reported to be more predominant and responsible for causing major fatalities in road accidents. Hence, frontal impact has been a widely studied subject in the field of occupant safety. Several ways of mechanical methods to absorb the impact energy have been tried in the past which were based mostly on friction and plastic deformation[5].

1.1 Importance of Deceleration during a Frontal Collision

In the current context of energy absorption during a frontal collision, head injury due to the deceleration is a major risk for the occupants. To quantify this injury, head injury criteria (HIC) has been formulated and is given as:

$$HIC = \max\left(t_2 - t_1\right)\left(\frac{1}{t_2 - t_1}\int_{t_1}^{t_2} a\left(t\right)dt\right)^{2.5} < 1000 \qquad (1)$$

where t_1 and t_2 are the initial and final time durations during the pulse for which *HIC* attains a maximum value and $\alpha(t)$ is the resultant acceleration. The current standard suggests that the HIC values above 1000 will induce an irrecoverable damage on head or brain[6]. It may be understood from Eqn. (1) that the acceleration (i.e. deceleration) during the impact is directly related to the probability of head injuries; and the initial peak crush force being the source of high intensity deceleration is a very critical factor from the occupant safety perspective. Further, an EAS should always be characterised by crush forces within the human tolerance limits. The maximum allowable deceleration[7] for a serious but not life-threatening injury is 20g.

1.2 Assessment Criteria for Energy Absorption

The total energy absorbed (TEA) by an EAS alone is not the direct measure of its crashworthiness. There are several other underlying parameters that are critical to the occupant safety. These parameters are quantifiable, help in assessing the crashworthiness and provide a deeper understanding of the crashworthiness of an EAS[8-11]. In summarizing the crashworthiness performance evaluation parameters, it is said that no single parameter can decide the efficacy of an EAS. An ideal EAS should absorb maximum energy with higher SE and CFE with a minimum mass. The crashworthiness assessment parameters are as given below.

Initial peak crush force (F_{peak}): It is the peak impact crush force that is required to trigger the plastic deformation in the structure. It should be within the threshold limits (equivalent acceleration levels ≤ 20 g to avoid serious injuries). The structure should exhibit an optimum F_{peak} whose accelerations are within the human tolerance limits and with a smooth time gradient to reach the first peak force.

$$F_{peak} = \max\left[F(x)\right] \tag{2}$$

where $F(x)$ is the instantaneous axial crush force at a crush distance of x.

Stroke efficiency (SE): It is the ratio of the length of an EAS (l) crushed by plastic deformation (i.e. effective crush stroke) to its initial total length (L). It is a fundamental performance indicator which influences other measures. Higher SE maximises TEA and helps in delaying the transfer of decelerations into the passenger cell. The SE is quantified as given below.

$$SE = \frac{l}{L} x100 \tag{3}$$

Total energy absorbed (TEA): It is the total energy absorbed by an EAS by plastic deformation during the impact. It is the area under the crush force (F) versus crush stroke (δ) curve. Theoretically, an EAS with nearly 100 % CFE (crush force efficiency) and SE can maximise TEA. The TEA during plastic deformation of an EAS is expressed as

$$TEA = \int_0^l F(x)dx \tag{4}$$

Crush force efficiency (CFE): It is the ratio of mean crush force (F_{mean}) to the F_{peak}. The crush force curve generally drops after F_{peak} and follows a series of fluctuations. For effective energy absorption, the crush force should tend to be uniform around the threshold value (equivalent acceleration ≤ 20g). It is not a direct measure of crashworthiness, but is a measure of stability of crush force that maximizes the TEA. The TEA by the structure will be maximum if CFE approaches unity. The CFE is expressed as

$$CFE = \frac{F_{mean}}{F_{peak}} x100 \tag{5}$$

Mean crush force (F_{mean}): It is expressed as

$$F_{mean} = \frac{TEA}{l} \tag{6}$$

Specific energy absorption (SEA): It is the ratio of the TEA by an EAS through plastic deformation to its total mass (m). The ideal requirement is to absorb a maximum amount of impact energy with a minimum possible mass of the EAS. In today's automotive industry, structures with superior performance-to-weight ratio are highly appreciated. The SEA is expressed as

$$SEA = \frac{TEA}{m} \tag{7}$$

1.3 Review of Geometric Cross-Sections for Energy Absorption

The existing structural configurations for crash energy absorption uses circular tubes, inversion of tubes, axial splitting of tubes, tube expansions, foam filled tubes, tubes with multi-cornered cross sections (i.e square or polygon), tubes with multi-cell configurations, frusta and conical tubes, composite tubes, etc. It is observed that the variations in combinations of tube thickness, perimeter of cross-section and material parameters (yield strength and young's modulus) for the same shape exhibit diverse deformation patterns making the subject of impact plasticity more complex and sensitive[12-15].

Different geometries and plastic deformation modes: Crush tubes with circular cross-sections have been widely studied for crash energy absorption due to their higher SE, ease of manufacturing and a wide variety of plastic deformation modes. Axial crush is the most common mode of plastic deformation and it has been observed that geometric parameters, i.e., diameter and thickness (d/t ratio) have a significant influence on the plastic deformation pattern and crush force behaviour[13,16]. Circular tube expansion has been proven to be ideal with a uniform crush force behaviour throughout the stroke[17] along with the method of axial splitting of tubes[18,19]. However these two methods are far from application as they require some special setup of die and guide to enable the special plastic deformation process. Nevertheless, another peculiar mode of plastic deformation i.e., inversion of circular tubes and frusta have been learnt to be a near-ideal crush force behaviour with CFE and SE tending to unity, but limited to only certain grades of metals with high degree of ductility[20-24].

Polygonal cross-sections: The deformation modes of tubes with square cross-sections are different to that of circular tubes because of their shape. Similar to circular tubes, geometric parameters play an influencing role in the

plastic deformation pattern and the crush force behaviour. Thin square tubes with high c/t ratio (where *c* is the side of the square and *t* is the thickness of the tube) i.e. higher than 50-60 are said to undergo non-compact collapse mode. On the other hand, square tubes with smaller *c/t* ratios (thick tubes) tend to deform with gradual and regular alternate inward and outward folds on successive faces of the tube. Moderate SE[25-27] work against these cross-sections. If the cross-section is made to be unconventional such as the shape of the mathematical operator 'plus' (+), the crush force behaviour is observed to be completely in contrast to a regular polygon with a F_{peak} followed by fluctuations in a narrow band as observed in the case of square tubes. However, the SE continues to be an issue with a premature densification[28-29].

Multi-celled configurations: Multi-celled configurations demonstrate moderately uniform crush force behaviour after the first peak, but an early densification of the crushed material proves detrimental to the stroke efficiency thus affecting the TEA[30-32].

Novel configurations: Crush tubes filled with metal or polymer foams have been observed to improve the TEA. Compressive strength of foams can be controlled by tuning the relative density and crush force behaviours[33]. Some attempts have been made to increase the crush force levels of regular tubes with axial stiffeners, beads and corrugations to improve the TEA[34-36]. A novel configuration with two concentric tubes connected with helically arranged stiffeners has been explored for a near-uniform crush force behaviour[37]. In the same category, circular tubes with ellipsoidal dimples have been studied to control the F_{peak} and stabilize the crush force behaviour[38]. Cellular arrangement in 3D with a crush tube stiffened with plates arranged longitudinally at 90° to each other were attempted to reduce the fluctuations in the crush force behaviour[39]. Other novel approaches such as piece-meal energy absorption system for varying energy situations based on the impact velocity[40]; tailor-welded blank based configuration with a precise combination of material grade and thickness along the crush tube to control the crush force behaviour[41]; and thin-walled hierarchical lattice configurations with progressive deformation arrangements for controlling the crush behaviour[42] have provided impetus for this research.

Composite tubes: Composite materials have been used for energy absorption because of directional control of material strength. Several studies have been performed with CFRP and GFRP based materials to understand the influence of material and constructional parameters such as fiber orientation, layup sequence and laminae thickness[43-44], different triggering schemes and configurations in truncated cone shapes to control the F_{peak}[45-46], precise combination of composite tubes with polymer foams[47], fiber-metal laminates in the form of both metal-intensive and composite-intensive forms[44-48]. However, cost, manufacturing and integrity issues have been observed to be the major roadblocks for the mainstream application of composites in road vehicles.

1.4 Research Gaps and Observations

An extensive review reveals that control over F_{peak}, higher SE, and CFE with simplicity in structural integrity are the primary requirements of an EAS. The following gaps associated with the existing cross-sections led to the present research.

(i) F_{peak} : F_{peak} with deceleration > 30 g are unsafe from the occupant safety perspective[13-14, 45].
(ii) *CFE*: Unstable $F-\delta$ behaviour after the first peak with high fluctuations leading to CFE of around 50 % [25,30,46].
(iii) *SE*: Conflicting influence of geometric cross-section and material on plastic folding pattern limit the SE to 75% [28-29].
(iv) Lack of a comprehensive study covering all basic geometric cross-sections with a final objective of finding new cross-sections from combination of basic shapes.

Based on detailed literature review, it is understood that, for metal based EAS with conventional approach, it is imperative to have an all-inclusive understanding of the influence of geometric parameters (cross-section and dimensions) on the crush force behaviour and thus the overall crashworthiness. Hence, in the current work, a comprehensive study has been planned on the energy absorption phenomenon of crush tubes made of different cross-sections with emphasis on all the crashworthiness parameters to form a basis for the development of new EAS configurations.

2. PRESENT RESEARCH

The present research is divided into three parts. In the first part, FEA methodology using the FEA code ABAQUS[49] is established for simulation of axial impact of crush tubes and is validated with an experimental study. In the second part, this FEA procedure is used to study the deformation behaviour of crush tubes with cross-sections made of regular polygons (triangle to octagon) and circle followed by a comprehensive assessment of their crashworthiness based on standard parameters. In the third part, new cross-sections made of combination of basic geometric shapes are proposed to combine the merits of different basic geometric shapes and their crashworthiness is assessed as per the standard parameters.

3. EXPERIMENTAL VALIDATION OF FEA METHODOLOGY

3.1 Material

A cylindrical crush tube specimen of stainless steel SS304 grade is machined from a rod of diameter 60 mm to achieve an outer diameter D= 50.0 mm, thickness t = 3.0 mm and length L= 90.0 mm. The material properties evaluated from tensile tests as per ASTM standard[50] are: elastic modulus E = 210 GPa; yield strength σ_y=290 MPa; tensile strength σ_u= 600 MPa; and elongation at break =55 %. The stress-strain curve is shown in Fig. 1.

3.2 FEA Setup

The FEA setup is shown in Fig. 2(a). The crush tube is discretised using 4-node S4R type shell elements in ABAQUS[49] with an average element length of 1.0 mm and a total element count of approximately 16000. The average element size of 1.0 mm has been arrived at after completing mesh convergence studies with element sizes of 2.4 mm, 2.0 mm, 1.4 mm, and 1.0 mm keeping convergence in crush force-crush displacement curves as target. The results of FE models with 1.4 mm and 1.0

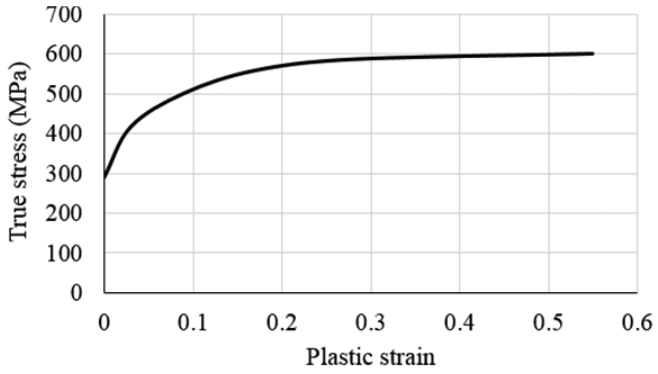

Figure 1. Stress-strain curve of stainless steel SS304 material.

mm element sizes were very similar and further, the deformation patterns of FE model with 1.0 mm element size were found to be close to those of the experiment. The bottom surface of the tube is fixed to the rigid ground structure which is represented with R3D4 type of rigid elements and the master node of the rigid connection is attached to the master node of the ground structure. The master node of the ground structure is completely constrained in all degrees of freedom. An intermediate top plate of size 80 mm x 80 mm and thickness 5 mm is placed at the top of the crush tube for load transfer. This intermediate top plate is also represented using S4R type shell elements with an average element size of 2 mm and is assumed to be made of linear elastic steel material. The impactor which is modelled using R3D4 type rigid elements is used to impact the intermediate plate. General contact algorithm is activated to capture all possible contact kinematics and behaviour. This contact algorithm activates contacts between different components on both positive and negative faces and also self-contact on either side of any component. Thus the contact algorithm captures all the realistic plastic deformations possible under the given axial impact scenario. Reference node of the impactor is left free in the axial direction and fixed in all other directions. An initial velocity of 0.1 mm/s is applied to the reference node of the impactor in the axial direction. The reaction forces in the axial direction at the ground surface are measured as the axial crush forces. The stress-strain behaviour of SS304 material shown in Fig. 1 is used in the analysis.

3.3 Experimental Setup

The observations from FEA are validated by conducting axial crush experiment. The experiment is conducted on a universal testing machine (UTM) with a load capacity of 250 kN as shown in Fig. 2(b). The tube specimen is kept on the test bed and the compressive load is applied through the intermediate plate at a quasi-static loading rate of 0.1 mm/s. The UTM's onboard computer gives the data of axial crush forces against the crush displacement.

3.4 Observations from FEA and Experiments

Comparison of deformation and crush force behaviours between FEA and experiment is shown in Fig. 3. The crushing starts with a high F_{peak} of 186 kN in FEA against 194 kN in the experiment to initiate the plasticity. The deformation process continues as a series of concertina folds. Progress

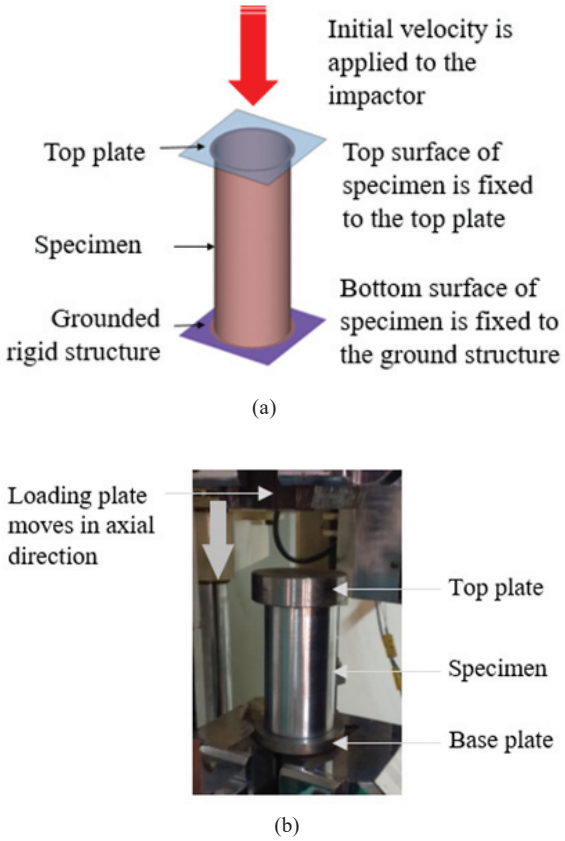

Figure 2. (a) FEA and (b) Experimental setups.

of deformation and $F-\delta$ response from FEA are shown in Figs. 3(a) and 3(c), respectively. The experimental deformation mode closely resembles the FEA as seen in Fig. 3(b). The $F-\delta$ behaviours of experiment and simulation match at a macro level, the difference being the secondary peaks in the case of experiment. No cracks are noticed in experiment agreeing with the FEA prediction of plastic strains within the elongation limits. It suggests that the FEA method largely represents the experiment in terms of deformation and $F-\delta$ behaviours thus validating the adopted FEA procedure.

4. BEHAVIOUR OF CRUSH TUBES WITH BASIC GEOMETRIC CROSS-SECTIONS

FEA of axial crushing of tubes with cross-sections of the following geometric shapes forms the first part of this study. The geometries considered are (a) Triangle, (b) Square, (c) Rectangle, (d) Pentagon, (e) Hexagon, (f) Octagon and (g) Circle. These geometric cross-sections with dimensions are shown in Fig. 4. Uniformity is maintained across all the specimens in terms of length, perimeter, mass and material. The common parameters are: L=240 mm, t =2.0 mm, perimeter = 360 mm, cross-sectional area = 720 mm^2, mass=0.5 kg and material is SS304. These specimens are subjected to axial crushing and their progress of deformation and $F-\delta$ behaviour are shown in Figs. 5 and 6, respectively.

4.1 Triangular Cross-section

The plastic deformation starts with an F_{peak} of 215 kN at $\delta \approx 4$ mm. The crush force then falls rapidly to 40 kN at

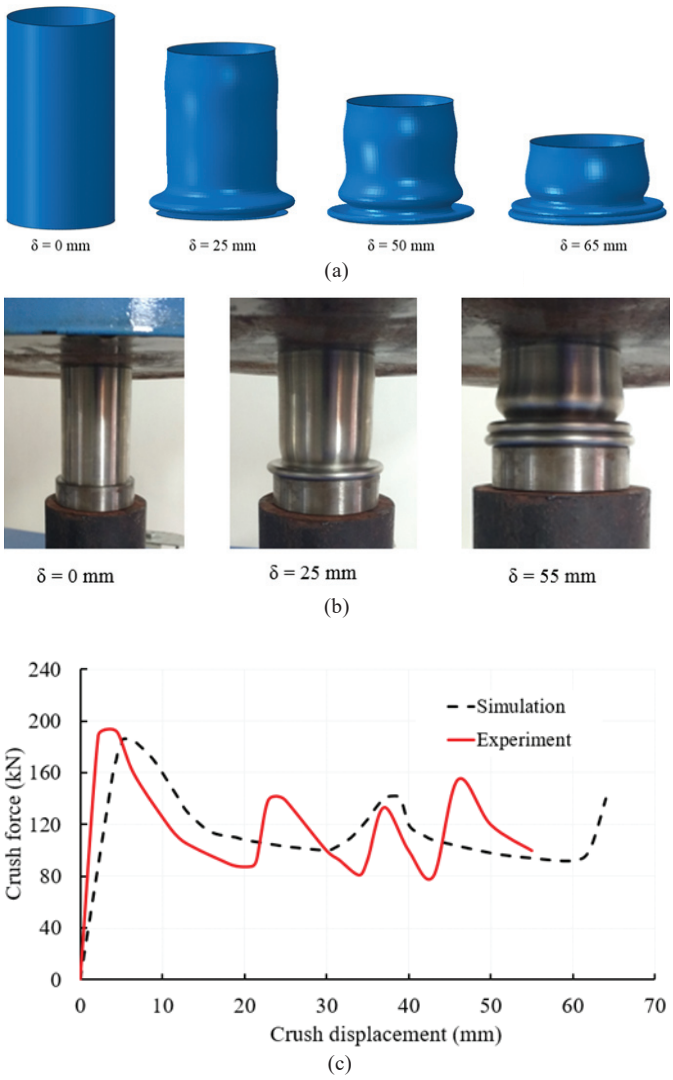

Figure 3. Deformation and *F*– δ behaviour of crush tube from FEA and experiment (a) Progress of deformation from FEA, (b) Progress of deformation from experiment, and (c) Crush force versus crush displacement.

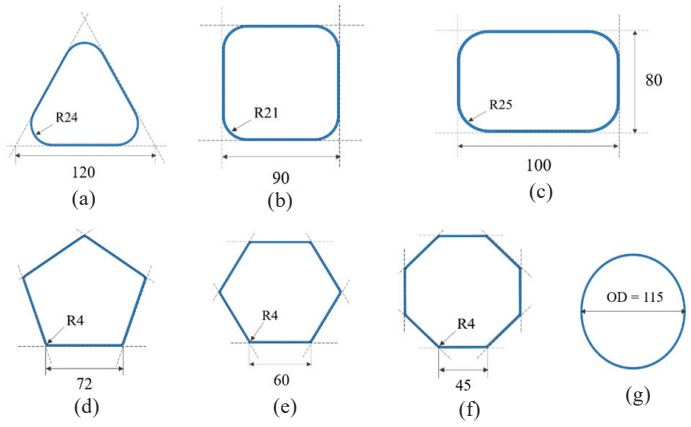

Figure 4. Crush tubes with different basic geometric shapes (dimensions in mm): (a) Triangle, (b) Square, (c) Rectangle, (d) Pentagon, (e) Hexagon, (f) Octagon, and (g) Circle.

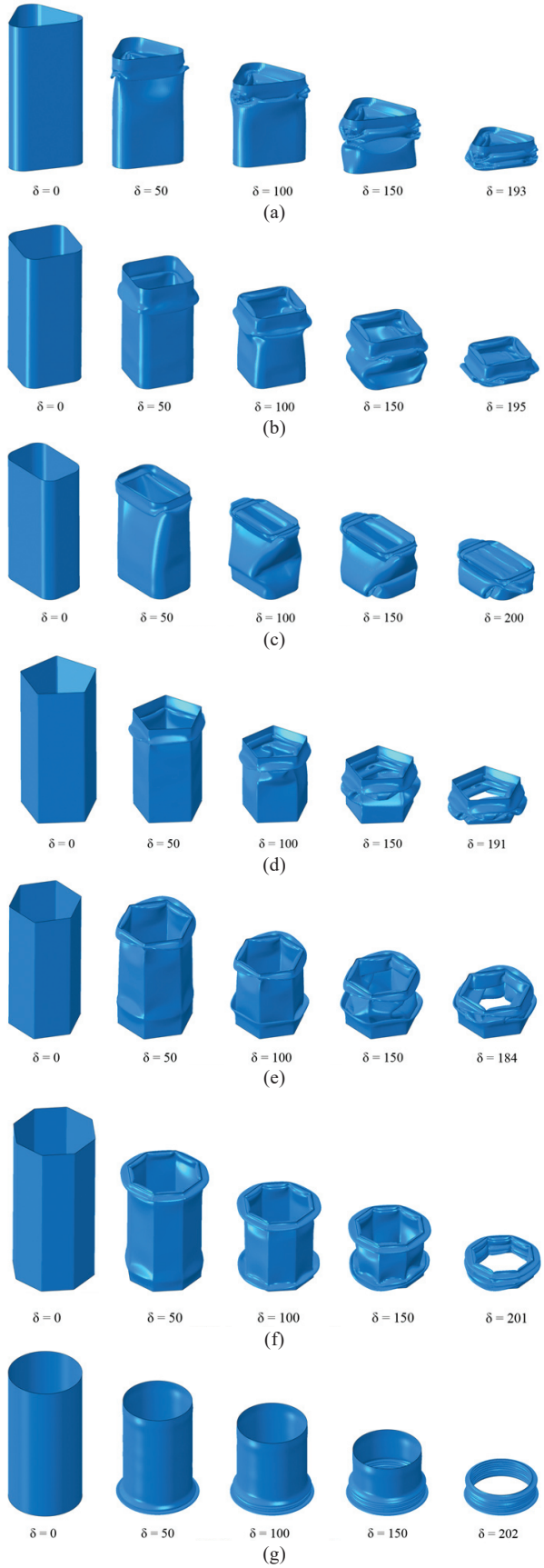

Figure 5. Progress of axial deformation of crush tubes specimens with different basic geometric cross-sections: (a) Triangular, (b) Square, (c) Rectangular, (d) Pentagonal, (e) Hexagonal, (f) Octagonal, and (g) Circular.

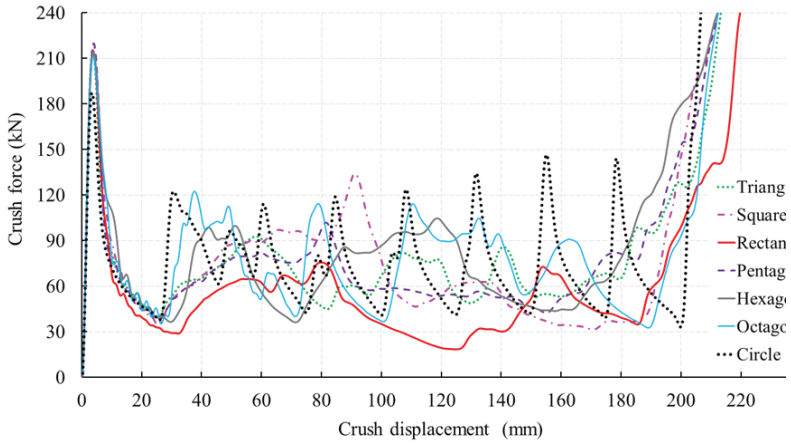

Figure 6. *F*– δ behaviour of crush tubes with all basic geometric cross-sections.

around δ =26 mm. During this period the section undergoes an inward fold on all the longitudinal faces of the tube. Further crushing brings an outward folding on all the faces, but this fold covers a longer envelope as it requires a longer longitudinal space to reverse the folding pattern from inner to outer face and this process happens over δ ≈ 60 mm. During this period, the crush force fluctuates between 40 kN and 90 kN with an equally spaced peak in the middle. Further crushing brings another inward fold with crush force fluctuating between 50 kN and 80 kN. The next outward fold brings the fluctuations within a range of 15 kN and the crush force stabilizes around 65 kN. Crushing ends at δ = 193 mm with TEA of 13.5 kJ.

4.2 Square Cross-section

The plastic deformation starts with an F_{peak} of 218 kN with outward folding on all faces of the tube and drops to 40 kN at δ≈24 mm at the end of the first fold. The second fold is observed to be inwards on all four faces of the tube. This transition between inward and outward folds demands higher crush forces of up to 130 kN spanning over a stroke of 80 mm. The third fold is a combination of outward and inward movements on alternate faces of the tube. Later, crush force settles at around 45 kN. Crushing ends at δ = 195 mm with TEA of 13.2 kJ.

4.3 Rectangular Cross-section

The first folding is observed to be outwards with an F_{peak} of 215 kN followed by a fall to 30 kN at δ = 36 mm ending the first fold. Due to unequal lengths of the adjacent sides in the cross-section, the longer side tends to flex in the outward direction to attain stable configuration. To balance this, the shorter side tends to move inwards interfering with the outward folding of the longer side. This conflicts results in a longer span of the fold making the structure weak against axial crushing resistance and the crush force drops below 20 kN. This pattern of low crush forces is completely in contrast to the earlier profiles. Crushing extends till 200 mm as the outward movement of longer side offers more space for crushing and absorbs an energy of 10.3 kJ. The *F*–δ behaviour appears stable for major part of the stroke, but with low magnitudes.

4.4 Pentagonal Cross-section

The first fold is observed to be outside with an F_{peak} of 220 kN followed by a drop to 38 kN at δ=25 mm. The second fold follows the trend of square profile with an alternate inward and outward movements on each successive face of the pentagon. As the cross-section has equal sides, the conflict between each successive face is reasonably balanced ensuring stability in crush force for about 140 mm of stroke after the F_{peak}. This is a contrasting feature in comparison to the earlier geometric shapes. However, uneven folding patterns caused internal contacts limiting the crushing to a moderate 191 mm absorbing an energy of 12.9 kJ.

4.5 Hexagonal Cross-section

This profile required an F_{peak} of 214 kN to initiate the first fold followed by a drop to 37 kN at about δ=31mm. First fold progresses inwards on all faces of the tube. During the second round fold, simultaneous outward folds are initiated next to the first fold region and at the other end of the tube, rising the crush force to around 90 kN. The crush force fluctuates until δ=175 mm. During this period alternate and conflicting inward and outward folds are observed on adjacent faces. This excessive deformation on both sides of the cross-section limits the crushing to a mere 184 mm resulting in the TEA of 13.2 kJ as the crush force operates at relatively higher magnitudes.

4.6 Octagonal Cross-section

This specimen required an F_{peak} of 211 kN to initiate the first fold which moves inwards completing the fold at δ=27 mm. Second fold is also observed to be inward but at the other end of the tube. This deformation pattern continues as a series of outward folds similar to concertina rings in the crushing of a circular tube[6-7]. The crush force fluctuates in a wide range between 40 kN and 110 kN. Crushing is active for 201 mm as no conflicts are observed in deformation modes absorbing 15.1 kJ of energy due to higher levels of crush forces and longer crush stroke.

4.7 Circular Cross-section

This required an F_{peak} of 187 kN for the first plastic fold, which is less compared to the previous cross-sections, as the continuity in cross-section profile limits the crushing resistance. Deformation progresses in a series of outward concentric folds. Each fold is characterised by a steep rise and fall in the crush force at the end of the fold with wild fluctuations in the crush force. The peak force of each ring fold keeps increasing as crushing progresses. Active crushing ends at δ=202 mm resulting in the TEA of 14.8 kJ.

4.8 Summary of Crush Behaviour of all Geometric Cross-sections

The *F*– δ behaviour of crush tubes with all geometric shapes is shown in Fig. 6 and detailed assessment of crashworthiness is given in Table 1.

Table 1. Crashworthiness assessment summary of all basic geometric cross-sections

Basic cross-section	F_{peak} (kN)	F_{mean} (kN)	Equivalent acceleration (g)	TEA (kJ)	δ (mm)	CFE (%)	SE (%)	SEA (kJ/kg)
Triangle	215	69.9	43.8	13.5	193	32.5	80.4	27.0
Square	218	67.7	44.4	13.2	195	31.0	81.3	26.4
Rectangle	215	51.5	43.8	10.3	200	23.9	83.3	20.6
Pentagon	220	67.5	44.8	12.9	191	30.7	79.6	25.8
Hexagon	214	71.7	43.6	13.2	184	33.5	76.7	26.4
Octagon	211	75.1	43.0	15.1	201	35.6	83.8	30.2
Circle	187	73.3	38.1	14.8	202	39.2	84.2	29.6

From this comparative study, the following inferences are drawn.

- High F_{peak} is a common drawback among all cross-sections;
- Conflict exists between CFE and SE;
- Quantitatively circular cross-sections exhibit superior crashworthiness, but fluctuations in crush forces is not a desirable trait; and
- Polygonal cross-sections display better stability in crush force behaviour after F_{peak}, but fail in CFE and SE due to instabilities at the later stages.

5. CROSS-SECTIONS WITH COMBINATION OF BASIC GEOMETRIC SHAPES

Taking vital clues from observations on detailed crashworthiness assessment of various geometric shapes, it can be noted that no single cross-section shape can demonstrate all-round crashworthiness. Hence, new cross-sections with combination of basic geometric shapes have been formed to exploit merits associated with each geometric shape. This is accomplished in two ways:

(i) Hybrid cross-section with a combination of circular arcs and straight lines constant throughout the length and

(ii) Lofted geometry with continuously varying cross-section with different basic cross-sections at each end.

5.1 Hybrid Cross-Section

5.1.1 Geometry of Cross-section

Geometric details of this hybrid cross-section are shown in Fig. 7(a). The purpose of linear segment is to add more strength to semi-circular tubes during crushing and to offer stability to the crush force by controlling fluctuations. This cross-section is constructed to understand the effect of cross-section shape on crashworthiness. The front flange corners are rounded with a fillet radius of 12 mm to minimise F_{peak}.

5.1.2 Analysis of Crash Performance

Progress of deformation of hybrid cross-section is shown in Fig. 8(a) and *F*–δ is shown in Fig. 9. This configuration required an initial F_{peak} of 153 kN, (equivalent acceleration of 31.2 g), followed by a series of fluctuations in the crush force from 153 kN at δ=14 mm to

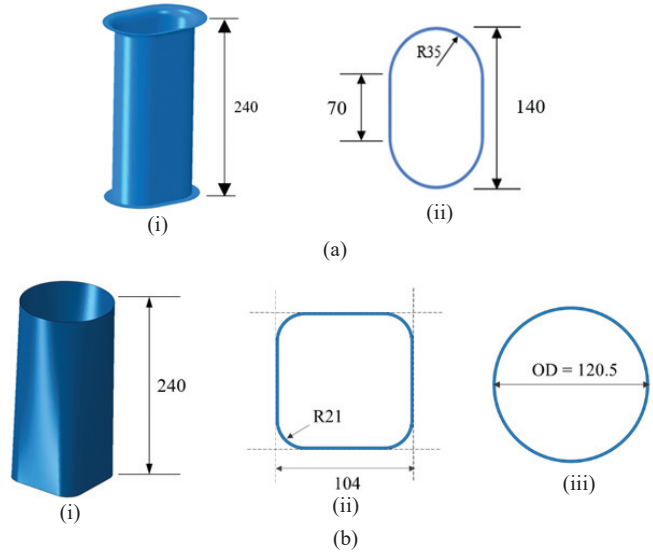

Figure 7. Geometry and constructional details of crush tubes formed by combination of basic geometric shapes (a) Hybrid crush tube specimen : (i) Geometry, (ii) Cross-section and (b) Square-to-circle lofted crush tube specimen : (i) Lofted crush tube, (ii) Bottom cross-section, (iii) Top cross-section.

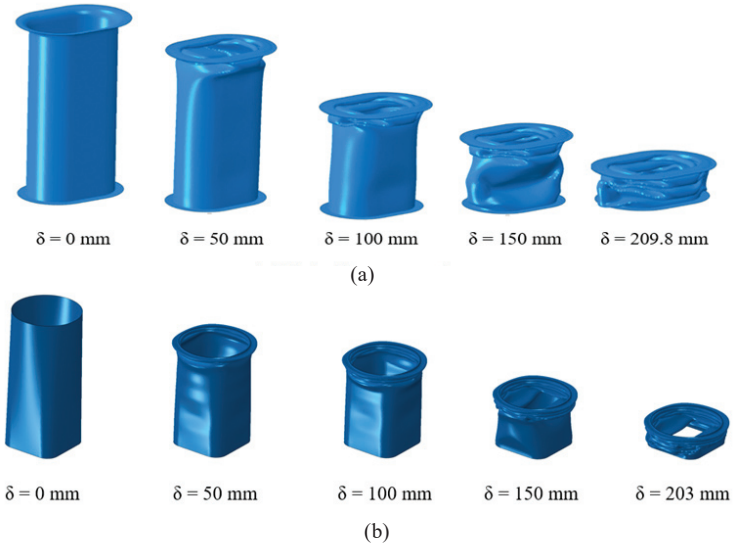

Figure 8. Progress of plastic deformation during axial crushing specimens formed by combination of basic geometric shapes (a) Hybrid cross-section and (b) Square-to-circle lofted cross-section.

60 kN at δ=29 mm. The crush force fluctuates in cycles with a span of around 24 mm for the first two cycles and the span increases with the crushing. Crush force tends to stabilise as crushing progresses from δ = 140 mm onwards. The crush force drops to 60 kN as the change in cross-section induces instability. However, crush force settles at 60 kN and crushing ends at a stroke of 210 mm taking SE to 84.2 %. This deformation pattern is different from both of circular and rectangular cross-sections when compared separately and this hybrid cross-section exhibits a superior performance in all crashworthiness parameters as shown in Table 2.

5.2 Lofted Geometry with Varying Cross-Section

5.2.1 Geometry of Cross-section

In this geometry, the topology of the crush tube is formed by lofting surfaces between a circle and a square at each end as shown in Fig. 7(b). Two different cross-sections provide a varying cross-section throughout the length inducing deviations in deformation patterns from those of basic circular and square tubes. Circular cross-section is placed at the impacting end of the tube as the F_{peak} of circular tube was observed to be lesser than the square tube as seen in Table 1.

5.2.2 Analysis of Crash Performance

Progress of deformation and F– δ curve are shown in Figs. 8(b) and 9, respectively. This deformation pattern is different from those of basic circular and square cross-sections in isolation. This geometry required an initial F_{peak} of 186 kN, (equivalent acceleration of 37.9 g) followed by a series of fluctuations in the crush force. The F– δ curve suggests that crush force behaviour deviates from that of the standard circular tube from the first fall after the initial peak which is observed to be around 50 kN against 36 kN of circular tube. This may be due to resistance from the varying cross section which changes from circular to square as the crushing progresses. The conflict between circular concertina deformation mode and that of the square tube controls the fluctuations in the crush force and keeps it between 60 kN and 80 kN for a longer stroke. This is in contrast to the F– δ and deformation pattern of a circular tube. On the other side, alternate inward-outward large folds on the adjacent faces observed in crushing of standard square tube are controlled to an extent in this variant. This tendency in the lofted variant helped in controlling the fall of crush force levels which was observed in the square tube. This lofted geometry combines the merits of basic circular and square cross-sections significantly bringing stability in the crush force. High F_{peak} can be controlled by suitable crush triggers. Higher SE of 84.5% and TEA of 15.42 kJ are superior to all the basic cross-sections.

5.3 Observations from Analysis of Hybrid and Lofted Cross-Sections

Comparison of F– δ behaviours and TEA trends of new geometries along with basic square and circular cross-sections is shown in Fig. 9 and their detailed assessment of crashworthiness is given in Table 2.

The hybrid cross-section exhibits deformation trait similar to that of the circular tube, may be due to dominant role of the circular arcs than the straight edges. Quantitatively, it demonstrates superior crashworthiness with higher TEA, but fails in maintaining the crush forces within the limits. The square-to-circle lofted geometry exhibits better control over the crush forces with a balance between deformation patterns of circle and square. Though this configuration scores low among two new geometries, it demonstrates its quality by absorbing the comparable amount of energy with crush force magnitudes within the limits after the initial peak, which is a superior feature of an EAS. High F_{peak} can be addressed by employing suitable crush triggers. Thus the varying cross-sectional topology shows good promise as a mainstream choice for EA applications and deserves further studies.

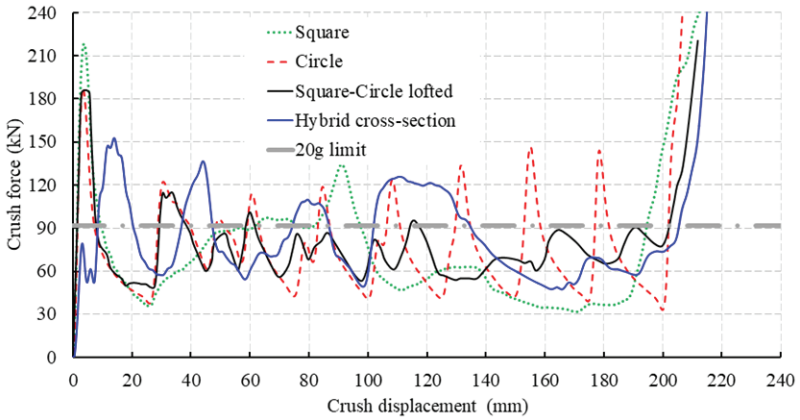

Figure 9. Comparison of crush behaviours of tubes with square, circle, hybrid and square-to-circle lofted cross-sections.

Table 2. Crashworthiness assessment of hybrid and lofted cross-sections and comparison with basic circular and square cross-sections

Cross-section	F_{peak} (kN)	F_{mean} (kN)	Equivalent acceleration (g)	TEA (kJ)	δ (mm)	CFE (%)	SE (%)	SEA (kJ/kg)
Square	218	67.7	44.4	13.2	195	31.0	81.3	26.4
Circle	187	73.3	38.2	14.8	202	39.2	84.2	29.6
Hybrid cross-section	153	84.2	31.2	17.7	209.8	55.0	87.5	35.4
Square-to-circle lofted	186	75.9	37.9	15.4	203	40.8	84.5	30.8

6. CONCLUSIONS

This paper studied the effect of geometric cross-sections on crashworthiness of crush tubes through numerical simulations. Based on crush performance of basic geometries, two new crush tube geometries based on hybrid cross-section and square-to-circle lofted cross-section have been proposed. No two specimens exhibited the same trends in crush force behaviour or deformations. The following conclusions can be drawn from this study.

- Cross-sections with equal cross-sectional areas exhibit almost the same initial F_{peak} .
- Polygonal (regular) cross-sections are favourable for stability in the crush force behaviour than the circular cross-sections.
- Circular or curved cross-sections are favourable for higher SE, but have high fluctuations in the crush forces.
- Regular polygonal cross-sections with six or more sides tend to exhibit a crush behaviour which closely resemble that of the circular cross-section.
- For an optimum balance between stability in the crush force, CFE, SE and TEA, pentagonal or hexagonal cross-sections may be a preferred choice among the pure polygonal cross-sections.
- Quantitatively, the hybrid cross-sections exhibit better crashworthiness when compared with cross-sections made of basic shapes, but lag behind in qualitative terms of crashworthiness and may be considered as the second choice in the current series.
- Lofted geometries with continuously varying cross-sections can offer better control over deformation trends for enhanced crashworthiness. Hence, these variable cross-sections are recommended as the primary choice of energy absorption from this study.

REFERENCES

1. National Highway Traffic Safety Administration. Final regulatory impact analysis: amendment of FMVSS No. 208-Passenger car front seat occupant protection. Washington DC: US Department of Transportation. 1984.
2. Du, B.P.; Chou, C.C.; Fileta, B.B.; Khalil, T.B.; King, A.I.; Mahmood, H.F.; Mertz, H.J.; Wismans, J.; Prasad, P. & Belwafa, J.E. Automotive Applications Committee-American Iron and Steel Institute. Southfield, MI, USA, 2004.
3. Huang, M. Vehicle Crash Mechanics. CRC Press, 2002.
4. World Health Organization. Global Status Report on Road Safety, 2015.
5. Lu, G. & Yu, T.X. Energy absorption of structures and materials. Woodhead Publishing, Cambridge, England., 2003, pp.114-254.
6. Chou, C.C.; Howell, R.J. & Chang, B.Y. A review and evaluation of various HIC algorithms. *SAE Trans.,* 1988, **1**, 713-747.
7. Perrone, N. Biomechanical problems related to vehicle impact. Prentice Hall, NJ, USA, 1972.
8. Clemens, H.J. & Burow, K. Experimental investigation on injury mechanisms of cervical spine at frontal and rear-front vehicle impacts. *SAE Trans.,* 1972, **1**, 2779-2796.
9. Gabauer, D. & Thomson, R. Correlation of vehicle and roadside crash test injury criteria. *In* Proceedings of the 19th International Technical Conference on the Enhanced Safety of Vehicles (ESV), Washington DC, 2005, **6**, 6-9.
10. Ambrosio, J.A. Crashworthiness: Energy Management and Occupant Protection. Springer, 2014.
11. Salehghaffari; Tajdari, M.; Panahi, M. & Mokhtarnezhad, F. Attempts to improve energy absorption characteristics of circular metal tubes subjected to axial loading. *Thin-Walled Struct.,* 2010, **8**(6), 379-390. doi: 10.1016/j.tws.2010.01.012
12. Abramowicz, W. Thin-walled structures as impact energy absorbers. *Thin-Walled Struct.,* 2003, **41**(2-3), 91-107. doi: 10.1016/S0263-8231 (02)00082-4
13. Andrews, K.R.; England, G.L. & Ghani, E. Classification of the axial collapse of cylindrical tubes under quasi-static loading. *Int. J. Mech. Sci.,* 1983, **25** (9-10), 687-696. doi: 10.1016/0020-7403(83)90076-0
14. Sun, G.; Pang, T.; Xu, C.; Zheng, G. & Song, J. Energy absorption mechanics for variable thickness thin-walled structures. *Thin-Walled Struct.,* 2017, **118**, 214-228. doi: 10.1016/j.tws.2017.04.004
15. Zahran, M.S.; Xue, P.; Esa, M.S.; Abdelwahab, M.M. & Lu, G. A new configuration of circular stepped tubes reinforced with external stiffeners to improve energy absorption characteristics under axial impact. *Latin American J. Sol. Struct.,* 2017, **14**(2), 292-311. doi: 10.1590/1679-78253231
16. Tvergaard, V. On the transition from a diamond mode to an axisymmetric mode of collapse in cylindrical shells. *Int. J. Sol. Struct.,* 1983, **19**(10), 845-856. doi: 10.1016/0020-7683 (83)90041-0
17. Yang, J.; Luo, M.; Hua, Y. & Lu, G. Energy absorption of expansion tubes using a conical–cylindrical die: experiments and numerical simulation. *Int. J. Mech. Sci.,* 2010, **52**(5), 716-725. doi: 10.1016/j.ijmecsci.2009.11.015
18. Huang, X.; Lu, G. & Yu, T.X. Energy absorption in splitting square metal tubes. *Thin-Walled Struct.,* 2002, **40**(2), 153-165. doi: 10.1016/S0263-8231(01)00058-1
19. Reddy, T.Y. & Reid, S.R. Axial splitting of circular metal tubes. *Int. J. Mech. Sci.,* 1986, **28**(2), 111-131. doi: 10.1016/0020-7403(86)90018-4.
20. Aljawi, A.A. & Alghamdi, A.A. Inversion of frusta as impact energy absorbers. *In* Current Advances in Mechanical Design and Production VII*,* 2000, 1, 511-519. Pergamon Press New York. doi: 10.1016/B978-008043711-8/50052-0
21. Alghamdi, A.A; Aljawi, A.A, Abu-Mansour, T.M. & Mazi, R.A. Axial crushing of frusta between two parallel plates. *In* Structural Failure and Plasticity, Pergamon Press New York, 2000, 545-550. doi: 10.1016/B978-008043875-7/50217-3
22. Nagel, G.M. & Thambiratnam, D.P. Dynamic simulation and energy absorption of tapered thin-walled tubes under oblique impact loading. *Int. J. Imp. Eng.,* 2006, **32**(10),

1595-1620.
23. Nia, A.A. & Hamedani, J.H. Comparative analysis of energy absorption and deformations of thin walled tubes with various section geometries. *Thin-Walled Struct.,* 2010, **48**(12), 946-954. doi: 10.1016/j.tws.2010.07.003
24. Hou, S.; Han, X.; Sun, G.; Long, S.; Li, W.; Yang, X. & Li, Q. Multiobjective optimization for tapered circular tubes. *Thin-Walled Struct.,* 2011, **49**(7), 855-863. doi: 10.1016/j.tws.2011.02.010
25. Abramowicz, W. & Jones, N. Dynamic axial crushing of square tubes. *Int. J. Imp. Eng.,* 1984, **2**(2), 179-208. doi: 10.1016/0734-743X(84)90005-8
26. Reid, S.R; Reddy, T.Y. & Gray, M.D. Static and dynamic axial crushing of foam-filled sheet metal tubes. *Int. J. Mech. Sci.,* 1986, **28**(5), 295-322. doi: 10.1016/0020-7403 (86)90043-3
27. Reddy, T.Y. & Al-Hassani, S.T. Axial crushing of wood-filled square metal tubes. *Int. J. Mech. Sci.,* 1993, **35**(3-4), 231-246. doi: 10.1016/0020-7403(93)90078-9
28. Abbasi, M.; Reddy, S.; Ghafari, N.A. & Fard M. Multi-objective crashworthiness optimization of multi-cornered thin-walled sheet metal members. *Thin-Walled Struct.,* 2015, **89,** 31-41. doi: 10.1016/j.tws.2014.12.009
29. Liu, W.; Lin, Z.; He, J.; Wang, N. & Deng, X. Crushing behavior and multi-objective optimization on the crashworthiness of sandwich structure with star-shaped tube in the center. *Thin-Walled Struct.,* 2016, **108**, 205-214. doi: 10.1016/j.tws.2016.08.021
30. Mahmoodi, A.; Shojaeefard, M.H. & Googarchin, H.S. Theoretical development and numerical investigation on energy absorption behavior of tapered multi-cell tubes. *Thin-Walled Struct.,* 2016, **102**, 98-110. doi: 10.1016/j.tws.2016.01.019
31. Goel, M.D. Deformation, energy absorption and crushing behavior of single, double and multi-wall foam filled square and circular tubes. *Thin-Walled Struct.,* 2015, **90**, 1-11. doi: 10.1016/j.tws.2015.01.004
32. Najafi, A. & Rais, R.M. Mechanics of axial plastic collapse in multi-cell, multi-corner crush tubes. *Thin-Walled Struct.,* 2011, **49**(1),1-12. doi: 10.1016/j.tws.2010.07.002
33. Kavi, H.; Toksoy, A.K. & Guden, M. Predicting energy absorption in a foam-filled thin-walled aluminum tube based on experimentally determined strengthening coefficient. *Mat. & Des.,* 2006, **27**(4), 263-269. doi: 10.1016/j.matdes.2004.10.024
34. Jones, N. & Birch, R.S. Dynamic and static axial crushing of axially stiffened square tubes. *Proceedings of the Inst. Mech. Eng., Pt C: Mech. Eng. Sci.,* 1990, **204**(5), 293-310. doi: 10.1243/PIME_PROC_1990_204_110_02
35. Zhang, X. & Huh, H. Energy absorption of longitudinally grooved square tubes under axial compression. *Thin-Walled Struct.,* 2009, **47**(12), 1469-1477. doi: 10.1016/j.tws.2009.07.003
36. Eyvazian, A.; Habibi, M.K.; Hamouda, A.M. & Hedayati, R. Axial crushing behavior and energy absorption efficiency of corrugated tubes. *Mat. Des.,* 2014, **54**, 1028-1038. doi: 10.1016/j.matdes.2013.09.031
37. Zhang, Z.; Liu, S. & Tang, Z. Crashworthiness investigation of kagome honeycomb sandwich cylindrical column under axial crushing loads. *Thin-Walled Struct., 2*010, **48**(1), 9-18. doi: 10.1016/j.tws.2009.08.002
38. Yang, K.; Xu, S.; Zhou, S.; Shen, J. & Xie, Y.M. Design of dimpled tubular structures for energy absorption. *Thin-Walled Struct.,* 2017, **112**, 31-40. doi: 10.1016/j.tws.2016.12.003
39. Zahran, M.S.; Xue, P. & Esa, M.S. Novel approach for design of 3D-multi-cell thin-walled circular tube to improve the energy absorption characteristics under axial impact loading. *Int. J. Crash.,* 2017, **22**(3), 294-306. doi: 10.1080/13588265.2016.1258958
40. Esa, M.; Xue, P.; Zahran, M.; Abdelwahab, M. & Khalil, M. Novel strategy using crash tubes adaptor for damage levels manipulation and total weight reduction. *Thin-Walled Struct.,* 2017, **111**, 176-188. doi: 10.1016/j.tws.2016.11.018
41. Xu, F.; Sun, G.; Li, G. & Li, Q. Experimental study on crashworthiness of tailor-welded blank (TWB) thin-walled high-strength steel (HSS) tubular structures. *Thin-Walled Struct.,* 2014, **74**, 12-27. doi: 10.1016/j.tws.2013.08.021
42. Sun, F.; Lai, C. & Fan, H. In-plane compression behavior and energy absorption of hierarchical triangular lattice structures. *Mat. Des.,* 2016, **100**, 280-90. doi: 10.1016/j.matdes.2016.03.023
43. Mahdi, E.; Hamouda, A.A. & Sebaey, T.A. The effect of fiber orientation on the energy absorption capability of axially crushed composite tubes. *Mat. Des.* 2014, **56**, 923-928. doi: 10.1016/j.matdes.2013.12.009
44. Kalhor, R. & Case, S.W. The effect of FRP thickness on energy absorption of metal-FRP square tubes subjected to axial compressive loading. *Comp. Struct.,* 2015, **130**, 44-50. doi: 10.1016/j.compstruct.2015.04.009
45. Yan, L.; Chouw, N. & Jayaraman, K. Effect of triggering and polyurethane foam-filler on axial crushing of natural flax/epoxy composite tubes. *Mat. Des., 2*014, **56**, 528-541. doi: 10.1016/j.matdes.2013.11.068
46. Boria, S.; Scattina, A. & Belingardi, G. Axial energy absorption of CFRP truncated cones. *Comp. Struct.,* 2015, **130**, 18-28. doi: 10.1016/j.compstruct.2015.04.026
47. Wang, L.; Fan, X.; Chen, H. & Liu, W. Axial crush behavior and energy absorption capability of foam-filled GFRP tubes under elevated and high temperatures. *Comp. Struct.,* 2016, **149**, 339-350.

doi: 10.1016/j.compstruct.2016.04.028
48. Dlugosch, M.; Fritsch, J.; Lukaszewicz, D. & Hiermaier, S. Experimental investigation and evaluation of numerical modeling approaches for hybrid-FRP-steel sections under impact loading for the application in automotive crash-structures. *Comp. Struct.,* 2017, **174**, 338-347. doi: 10.1016/j.compstruct.2017.04.077
49. ABAQUS 6.14.3 Documentation, Dassault Systèmes Simulia Corp., Providence, RI, USA, 2014.
50. ASTM E8/E 8M-08, Standard Test Methods for Tension Testing of Metallic Materials, American Society for Testing Materials, 2008.

CONTRIBUTORS

Dr Thokala Janardhan Reddy has recently completed PhD from BITS-Pilani, Hyderabad.
In the present study, he has conceived various geometries of crush tube structures for crash energy absorption in the road vehicles and conducted FEA simulations and experiments.

Dr Vijayabaskar Narayanamurthy is currently working as Scientist-F at Research Centre Imarat, Hyderabad.
In the present study, he has guided the research work on virtual validation using FEA tools and experiments.

Dr Venkata Daseswara Rao Yendluri has a PhD in mechanical engineering from NIT, Raipur.
In the present study, he has guided the research work on formulation of the problem from the structural mechanics perspective.